

# TIMING OF HEAVY ION COLLISIONS AT SIS ENERGIES\*

H. OESCHLER

for the KaoS Collaboration

Institut für Kernphysik, Technische Universität Darmstadt  
D-64289 Darmstadt, Germany

(Received December 7, 1999)

A review of pion emission in heavy ion collisions is given and it is discussed whether these spectra and the various particle yields can be interpreted within a thermal model with an emission at a unique temperature. A careful inspection of the high-energy pions reveals that they are emitted during the early phase of the collisions while pions with lower energies are emitted mainly later and over a long time interval.

PACS numbers: 25.75.-q, 25.75.Dw

## 1. Introduction

Central heavy ion collisions at relativistic energies represent an ideal tool to study nuclear matter at high densities and at high temperatures. However, these collisions are rather complex. An understanding of their time evolution is needed before detailed information can be extracted. Pions are the most abundantly produced particles at relativistic energies. Due to their high interaction cross section with nuclear matter they are continuously “absorbed” by forming baryonic resonances (*e.g.*  $\pi N \rightarrow \Delta$ ) which then decay again into pions. Therefore, pions can be emitted from the first interactions until a very late stage of the collision.

An overview of the measured pion spectra is given in the first part. These results are discussed along with the question whether the observations are in agreement with the assumption of a thermal and chemical equilibrium. The second part addresses the question of the origin of high-energy pions. Here, it will be shown that pion emission is a time-dependent process.

---

\* Invited talk presented at the XXVI Mazurian Lakes School of Physics, Krzyże, Poland, September 1–11, 1999.

## 2. Pion spectra

The experiments were performed using the Kaon Spectrometer [1] at the heavy-ion synchrotron SIS at GSI (Darmstadt). For details see Ref. [2].

Data on pion spectra up to laboratory momenta of 1400 MeV/c have been measured in mass symmetric systems from A= 12 to A= 197 and at incident energies from 0.6 to 2.0 A · GeV. As a representative selection, Fig. 1

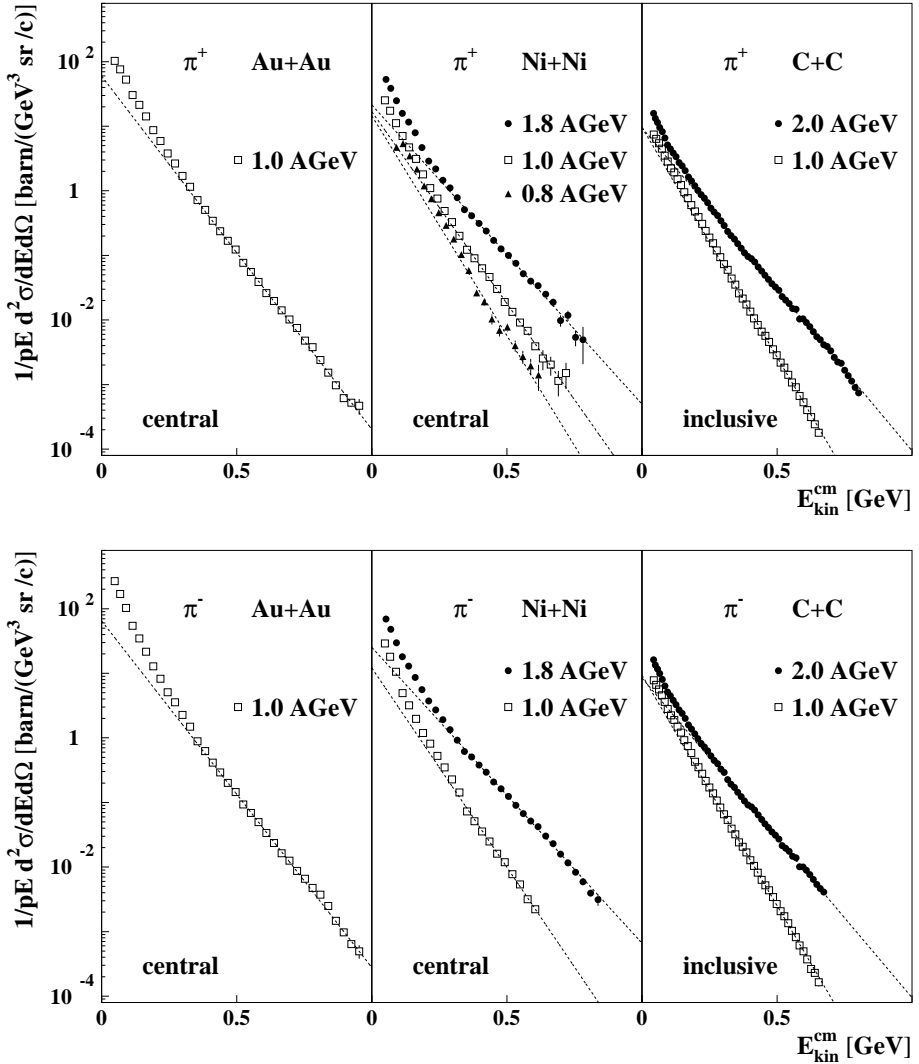


Fig. 1. Spectra of positively and negatively charged pions in the center-of-mass frame in a “Boltzmann” representation for various reactions (preliminary data).

shows double differential cross sections of positively and negatively charged pions in the Boltzmann representation  $1/(pE) \times d^2\sigma/(dEd\Omega)$  for various mass systems and at different incident energies. The spectra are measured at laboratory angles corresponding to a center-of-mass angular range within  $90 \pm 30$  degrees.

All spectra exhibit concave shapes in this representation. Straight lines (Boltzmann distributions) fitted to the high-energy tail, *i.e.* to kinetic energies above the corresponding to the limit for free  $NN$  collisions, are shown. The inverse slope parameters increase with incident energy and with increasing mass of the collision system. The inverse slope parameters of positively charged kaons are about the same, those of protons are always higher as shown in Ref. [2].

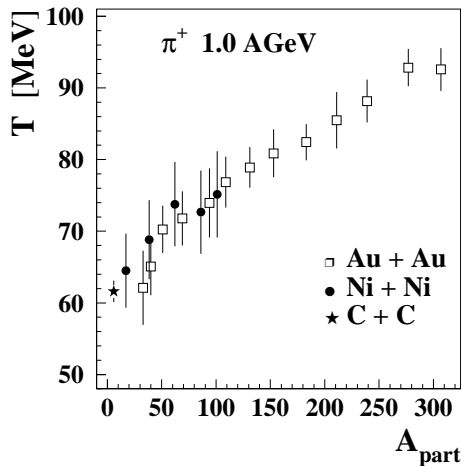


Fig. 2. The inverse slope parameters of the high-energy part of the spectra of positively charged pions for different collision systems reveal a very similar behaviour if plotted as a function of  $A_{\text{part}}$ .

It is of interest to study the variation of the slopes of the high-energy part of the pion spectra in further details by selecting various centrality regions, *i.e.* as a function of  $A_{\text{part}}$ . Figure 2 shows that the inverse slope parameters increase with  $A_{\text{part}}$ . It is interesting to remark that the values from all collision systems at 1 A·GeV fall on a common line. These findings together with the obtained slope parameters from participating protons fit into a picture of a thermal, radially expanding source. Since the influence of flow increases with the mass of the emitted particle, protons show higher “apparent temperatures”.

While kaons and protons exhibit Boltzmann-like spectra, pions show concave shapes as presented in Fig. 1. This can be understood by the fact

that pions are either “free” or “bound” in baryonic resonances. At freeze out the pion spectra are then composed of a “thermal” component and another one governed by the decay kinematics of the excited baryonic resonances. Indeed, the measured shapes (Fig. 1) can be qualitatively understood by such a scenario. Recent quantitative examples of such decompositions are found *e.g.* in Ref. [4,5].

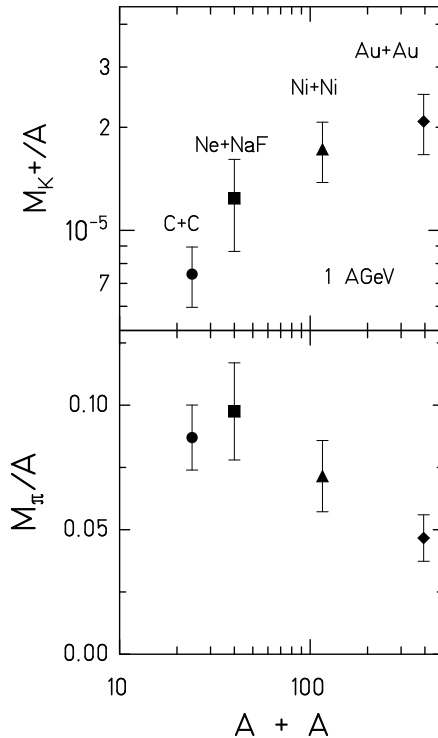


Fig. 3. Pion ( $\pi^+$ ,  $\pi^0$ ,  $\pi^-$ ) and  $K^+$  multiplicities per  $A$  as a function of  $A+A$ .

The spectra and their slopes presented so far are pointing towards the interpretation within a thermal concept. Therefore, we study next whether the yields can be understood within a thermal model. First, we show in Fig. 3 the measured multiplicities for pions and  $K^+$ . This figure evidences a strong contrast. While the pion multiplicity slightly decreases with the mass of the colliding system, the  $K^+$  multiplicity rises strongly. The latter observation seems to be in conflict with a thermal interpretation, which — in a naive view — should give multiplicities per  $A$  being constant.

The production of strange particles obviously has to fulfill strangeness conservation. However, the usual grand-canonical treatment is not sufficient, if the number of strange particles is small. A thermal model has to

take care of exact strangeness conservation in each reaction. This is done by taking into account in the expression for the “weight function” that together with each  $K^+$  also another particle, *e.g.* a  $\Lambda$  is produced. This extension has been done recently and leads to a reduction of  $K^+$  as compared to the numbers without exact strangeness conservation [6]. In the low-number limit, the additional term leads to a linear rise of  $M_{K^+}/A$  or a quadratic rise of  $M_{K^+}$  which is in remarkable agreement with the experimental observation as shown in Fig. 4, from [6].

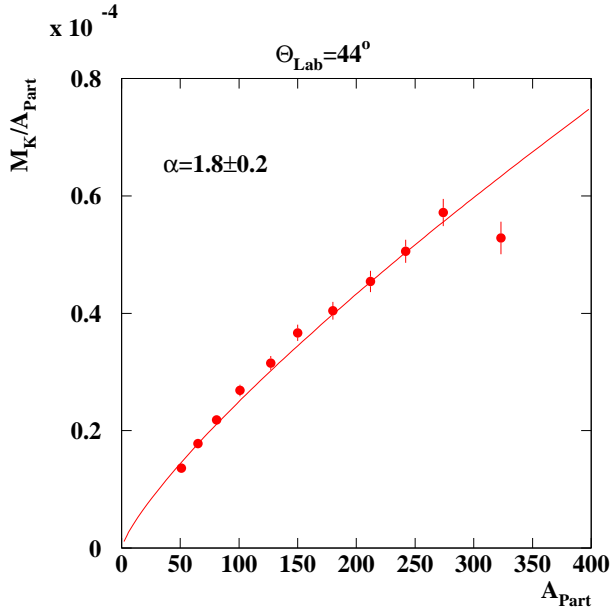


Fig. 4. The multiplicity of  $K^+/A_{\text{part}}$  rises strongly with  $A_{\text{part}}$  and this rise can be described by the thermal model including exact strangeness conservation [6].

The various measured yields (or particle ratios) lead in this thermal model to lines in the  $T - \mu_B$  plane. As an example, we show in Fig. 5 the various lines for Ni+Ni collisions. Besides the results for  $\eta/\pi_0$  all measured values cross at about one unique pair of  $T$  and  $\mu_B$ . Surprisingly, even the measured  $K^+/K^-$  ratio fits into this representation. This suggests that all particles freeze out with the same temperature. If one thinks of the expanding and cooling system, it implies a unique freeze-out time for all particles. In the next chapter, however, we will give arguments that this is questionable.

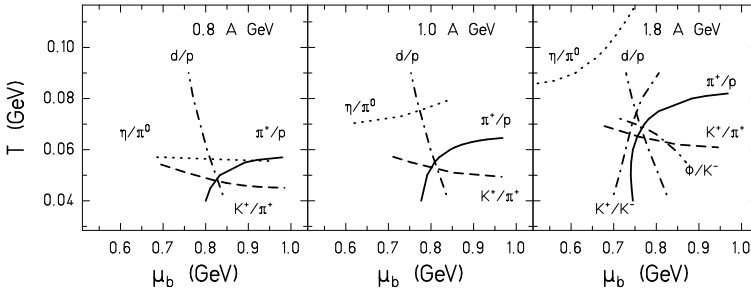


Fig. 5.  $T$  versus  $\mu_B$  for central Ni+Ni collisions from 0.8 A·GeV to 1.8 A·GeV. From [6] and new, preliminary data for  $K^+$  and  $K^-$  [7].

### 3. Time evolution of pion emission

A detailed interpretation of the pion spectra is still under debate. Many models, either thermal concepts or microscopic descriptions, have difficulties to describe the entire pion spectra properly. While there is little discussion on the rise of the low-energy part of the spectra (decaying baryonic resonances), the origin of the high-energy part of the pion spectra remains open. Here, independent observations are given which can be summarized as follows: High-energy pions are emitted at an early stage of the collision. This is based on:

- (i) Spectra of oppositely charged pions emitted in central Au+Au collisions at 1.0 A·GeV are compared [8]. The  $\pi^-/\pi^+$  difference is attributed to the influence of isospin and Coulomb field. This allows to extract the effective Coulomb field at the instant of the pion emission as the isospin effect is known. It turns out that a constant Coulomb potential  $V_{\text{Coul}}$  is unable to describe the difference between the spectra at all momenta as shown in Fig. 6. A rather weak  $V_{\text{Coul}}$  is needed to describe the low-energy part of the spectra; in contrast to the much stronger  $V_{\text{Coul}}$  needed for the high-energy part. The lower value of  $V_{\text{Coul}}$  for low-energy pions indicates a more dilute charge distribution.
- (ii) Direct experimental evidence for the time evolution of pion emission is presented based on the shadowing of spectator matter in certain space-time regions [9]. For this purpose we have chosen peripheral collisions of Au+Au at 1.0 A·GeV incident energy. The moving spectator matter acts like a shutter of a camera shielding the pion, *i.e.* modifying the pion emission pattern according to the spatial distribution of the spectator matter at the time of the pion freeze out. The motion of the spectator serves as a calibrated clock.

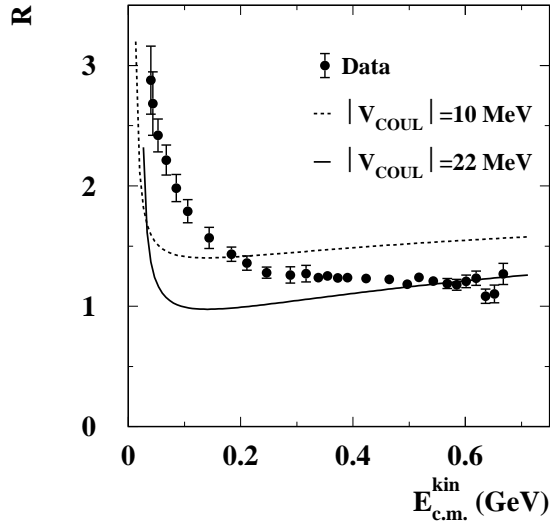


Fig. 6.  $\pi^-/\pi^+$  ratio for the reaction system  $^{197}\text{Au}+^{197}\text{Au}$  as a function of the pion kinetic energy for central collisions. The solid (dotted) curve shows the calculated ratio for a fixed Coulomb energy of 22 MeV (10 MeV). The error bars reflect statistical errors only; a systematic error of  $\pm 5\%$  has to be added.

A preferential emission perpendicular to the reaction plane has already been observed for this collision system [10,11]. Recently, an enhanced emission of pions opposite to the main direction of nucleons emission was observed [13]. This “antiflow” behaviour is found to be pronounced only in peripheral collisions. In this work we reveal the effects of “flow” and “antiflow” as resulting from the interplay of the time evolution of the pion emission with the shadowing of the surrounding matter.

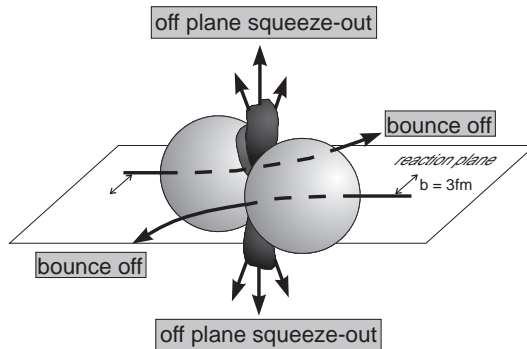


Fig. 7. Illustration of the geometrical situation of two colliding nuclei showing the reaction plane and out-of-plane emission (from [14]).

Figure 7 illustrates the emission in respect to the reaction plane. The orientation of the reaction plane is determined [11] using the recipe given by Danielewicz [15]. This procedure yields the so-called  $Q$ -vector which allows also to distinguish projectile and target side.

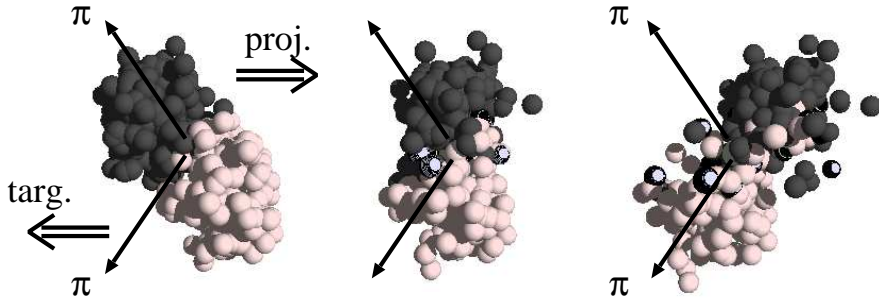


Fig. 8. Sketch of an Au+Au collision at 1 A·GeV with an impact parameter of 7 fm as calculated by a QMD transport code [12]. The snapshots are taken at 4 fm/c (left), 10 fm/c (middle) and 16 fm/c (right). The arrows indicate the direction of the spectrometer at target rapidity.

Figure 8 depicts the nuclear matter distribution for a Au+Au collision at a beam energy of 1 A·GeV at 4, 10 and 16 fm/c after the first touch of the nuclei. These pictures are the result of a transport calculation for an impact parameter of  $b = 7$  fm [12]. The snapshots sketch the effect of pion shadowing in the reaction plane by spectator matter at different stages of the collision. Those pions which are emitted in the early phase of the collision and which are detected around target rapidity (*i.e.* at backward angles as indicated by the arrows in Fig. 8) will be shadowed by the projectile spectator on one side and therefore exhibit “flow” to the other side. In contrast, if pions freeze out at a late stage of the collision they will be shadowed (at target rapidity) by the target spectator which results in an “antiflow”-like configuration. Experimentally, we compare the number of pions emitted in the reaction plane towards the side of the projectile spectator  $N(\phi = 0^\circ)$  with the number of those pions emitted into the opposite direction  $N(\phi = 180^\circ)$ . The azimuthal angle  $\phi = 0^\circ$  is defined by the projectile.  $N_\pi(0^\circ)$  refers to the angular range of  $-45^\circ < \phi < 45^\circ$ , and  $N_\pi(180^\circ)$  to the angular range of  $135^\circ < \phi < 225^\circ$ .

Figure 9 shows the ratio of these numbers for  $\pi^+$  and  $\pi^-$  mesons as a function of transverse momentum  $p_T$  in two different rapidity regions and for peripheral collisions. In all cases both  $\pi^+$  and  $\pi^-$  (open and full symbols) show a similar behavior ruling out Coulomb effects as the origin of the observed effect.

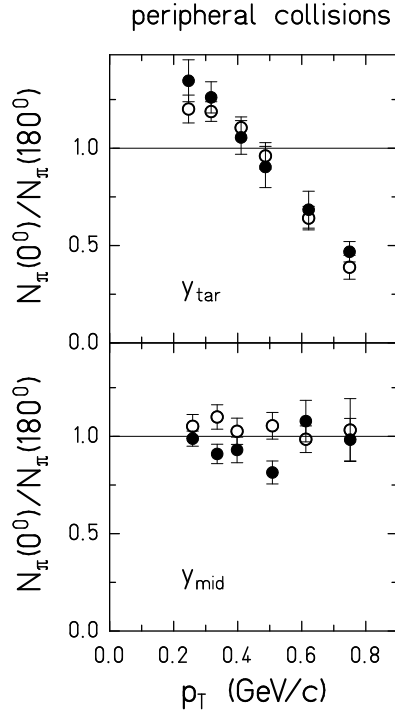


Fig. 9. Pion number ratios  $N_\pi(0^\circ)/N_\pi(180^\circ)$  as a function of transverse momentum.  $N_\pi(0^\circ)$  and  $N_\pi(180^\circ)$  denote the number of pions emitted towards the projectile and towards the target side, respectively. The spectra are measured in peripheral Au + Au collisions at 1 A-GeV and at two rapidity regions ( $0.01 \cdot y_{\text{beam}} \leq y_{\text{tar}} \leq 0.10 \cdot y_{\text{beam}}$  and  $0.44 \cdot y_{\text{beam}} \leq y_{\text{tar}} \leq 0.56 \cdot y_{\text{beam}}$ ). Full (open) symbols refer to  $\pi^-$  ( $\pi^+$ ) emission. Only statistical errors are shown.

At midrapidity the measured ratios are close to one as expected for symmetric systems. At target rapidity (upper panel of Fig. 9) the ratio  $N_\pi(0^\circ)/N_\pi(180^\circ)$  decreases from about 1.2 at low  $p_T$  values to about 0.5 at high  $p_T$ . This behavior corresponds to a transition from pion number antiflow to flow with increasing transverse momentum. In earlier measurements [13] it has been integrated over pion momentum and hence, pionic antiflow has been found since the pion yield is dominated by low-momentum pions. The transition from antiflow to flow as a function of transverse momentum shown in the upper left panel of Fig. 9 is a new observation which will be discussed in more details along with Fig. 10.

A more detailed picture of pion emission is obtained by comparing the yield of pions emitted in plane to the yield of pions emitted perpendicular to the reaction plane. The latter pions are expected to be much less af-

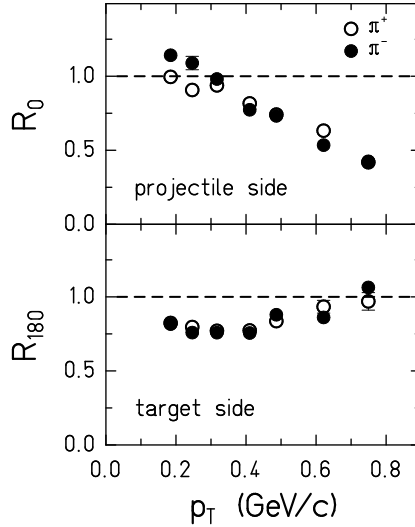


Fig. 10. Ratio of the pion spectra for in-plane emission to the one out of plane in peripheral Au+Au collisions at 1 A-GeV at target rapidities. The upper part refers to the emission towards the “projectile side”, the lower one towards the “target side”. Full (open) symbols refer to  $\pi^-$  ( $\pi^+$ ) emission.

affected by shadowing or rescattering by spectator matter and hence provide a nearly undisturbed view onto the pion source. In order to visualize the effect of shadowing for different pion momenta we normalize the “in-plane” pion spectra ( $N_\pi(0^\circ)$  and  $N_\pi(180^\circ)$ ) to the “out-of-plane” spectra ( $N_\pi(\text{perp}) = (N_\pi(90^\circ) + N_\pi(270^\circ))/2$ ).

Figure 10 shows the ratios  $R_0 = N_\pi(0^\circ)/N_\pi(\text{perp})$  (“projectile side”, upper panel) and  $R_{180} = N_\pi(180^\circ)/N_\pi(\text{perp})$  (“target side”, lower panel) as a function of transverse momentum for peripheral collisions and at target rapidities. The ratios  $R_{0,180}$  in Fig. 10 do not exceed unity. This indicates that the azimuthal asymmetry as shown in Fig. 9 is not caused by an enhanced pion emission but rather by losses due to absorption or rescattering. Figure 10 allows to extract detailed information on the emission time of pions as a function of their momentum. At pion momenta around 0.4 GeV/c, the upper left panel of Fig. 9 exhibits no asymmetry ( $N_\pi(0^\circ)/N_\pi(180^\circ) \approx 1$ ) whereas Fig. 10 clearly shows that pion emission into the reaction plane is depleted ( $R_{0,180} < 1$  both at the projectile and target side). This effect is expected if pions are emitted at about 10 fm/c when they are shadowed equally by either the target or the projectile spectator (see Fig. 8 middle part).

For pions with momenta above  $0.4 \text{ GeV}/c$ , the loss increases with increasing momentum for pions emitted towards the projectile side (upper panel of Fig. 10) whereas the opposite trend is observed for pions emitted towards the target side (lower panel of Fig. 10). This finding shows that pions with high momenta are correlated with early emission times (which are even shorter than  $10 \text{ fm}/c$ ). In contrast, low-energy pions predominantly freeze out at a later stage of the collision. This information is based on the observation that pions with momenta below  $0.3 \text{ GeV}/c$  suffer from absorption or rescattering when emitted towards the target side but remain rather undisturbed when emitted towards the projectile side. The depletion for low-energy pions is less pronounced than for high-energy pions (upper panel Fig. 10). This effect indicates that low-energy pions freeze out over an extended time span. Again,  $\pi^-$  and  $\pi^+$  mesons behave very similarly which demonstrates that the observed effects are not caused by Coulomb interaction.

Our data show that in Au + Au collisions at  $1 \text{ A}\cdot\text{GeV}$  most of the high-energy pions freeze out within  $10 \text{ fm}/c$  after the first touch of the nuclei. Transport models predict a similar time scale for the emission of high-energy pions [16, 17]. According to calculations, the nuclear density exceeds twice the saturation value in central Au+Au collisions at  $1 \text{ A}\cdot\text{GeV}$  within the first  $15 \text{ fm}/c$  [16].

#### 4. Summary

A global survey of the spectral shapes and yields of the emitted pions,  $K^+$  and protons points towards an interpretation within a thermal concept. This model takes into account exact strangeness conservation, *i.e.* the associate production of two strange particles (*e.g.*  $K^+$  and  $\Lambda$ ). It does not only explain the various particle ratios (except  $\eta$ ), but also describes the very different  $A_{\text{part}}$ -dependences of the  $K^+$  and  $\pi$  multiplicities.

However, a detailed inspection of the pion emission (comparison of  $\pi^+$ ,  $\pi^-$  emission and shadowing of pions by spectator matter in peripheral collisions) reveals that high-energy pions freeze out at an early stage of the collision, while the low-energy ones are emitted during the whole collision process.

The apparent discrepancy between the two parts of the paper seems to be closely related to the question, whether chemical and thermal freeze out are identical. This distinction has not been made carefully in the first part which mainly addresses the chemical freeze out. The latter part discusses the dynamical evolution of a “thermal” freeze out keeping in mind that it is open whether thermal equilibrium is reached at all.

The data presented have been measured and analyzed by the KaoS Collaboration: A. Förster, H. Oeschler, C. Sturm, F. Uhlig, A. Wagner (Institut für Kernphysik, Technische Universität Darmstadt, D - 64289 Darmstadt, Germany), P. Koczn, F. Laue, M. Mang, P. Senger (Gesellschaft für Schwerionenforschung, D-64220 Darmstadt, Germany), E. Schwab, Y. Shin, H. Ströbele (Johann Wolfgang Goethe-Universität, D-60325 Frankfurt/Main, Germany), I. Böttcher, B. Kohlmeier, M. Menzel, F. Pühlhofer (Philipps-Universität, D-35037 Marburg, Germany), M. Debowski, W. Walus (Jagiellonian University, PL-30-059 Kraków, Poland), F. Dohrmann, E. Grosse, L. Naumann, W. Scheinast (Forschungszentrum Rossendorf, D-01314 Dresden, Germany).

## REFERENCES

- [1] P. Senger *et al.*, *Nucl. Instrum. Methods* **A327**, 393 (1993).
- [2] C. Müntz *et al.*, *Z. Phys.* **A357**, 399 (1997).
- [3] M. Mang, Ph.D.thesis, University of Frankfurt, 1997.
- [4] A. Weinhold, B. Friman, W. Nörenberg, *Phys. Lett.* **B433**, 236 (1998).
- [5] A. Förster, master's thesis, Technische Universität Darmstadt, 1998.
- [6] J. Cleymans, H. Oeschler, K. Redlich, *Phys. Rev.* **C59**, 1663 (1999).
- [7] M. Menzel, Ph.D.thesis, University of Marburg, in preparation.
- [8] A. Wagner *et al.*, *Phys. Lett.* **B420**, 20 (1998).
- [9] A. Wagner, Ph.D.thesis, Technische Universität Darmstadt, 1997 and A. Wagner *et al.*, submitted to *Phys. Rev. Lett.*
- [10] D. Brill *et al.*, *Phys. Rev. Lett.* **71**, 336(1993).
- [11] D. Brill *et al.*, *Z. Phys.* **A357**, 207 (1997).
- [12] C. Hartnack, private communications.
- [13] J.C. Kintner *et al.*, *Phys. Rev. Lett.* **78**, 4165 (1997).
- [14] J. Konopka, Ph.D.thesis, University of Frankfurt, Germany, 1995.
- [15] P. Danielewicz, *Phys. Rev.* **C51**, 716 (1995).
- [16] S.A. Bass *et al.*, *Phys. Rev.* **C50**, 2167 (1994).
- [17] B.A. Li and W. Bauer, *Phys. Rev.* **C44**, 450 (1991).